Available online at www.sciencedirect.com
SCIENCE DIRECT®
Journal of Molecular Catalysis A: Chemical 220 (2004) 103–112
JOURNAL OF MOLECULAR CATALYSIS A: CHEMICAL
www.elsevier.com/locate/molcata

Microstructures of V-P-O catalysts derived from $VOHPO_4 \cdot 0.5H_2O$ of different crystallite sizes

Yuichi Kamiya [a], Norihito Hiyoshi [b], Naonori Ryumon [b], Toshio Okuhara [b,*]

[a] *Japan Science and Technology Corporation, 4-1-8 Honcho, Kawaguchi 332-0012, Japan*
[b] *Graduate School of Environmental Earth Science, Hokkaido University, Sapporo 060-0810, Japan*

Received 16 December 2003; accepted 3 March 2004

Abstract

The influence of crystallite size of precursor $VOHPO_4 \cdot 0.5H_2O$ on the microstructure of a resulting catalyst and selective oxidation of *n*-butane are investigated. Two kinds of $VOHPO_4 \cdot 0.5H_2O$, small crystallites (av. 1 μm × 110 nm) and large crystallites (av. 10 μm × 415 nm), were prepared by intercalation-exfoliation-reduction of $VOPO_4 \cdot 2H_2O$ in 2-butanol and the direct reduction of $VOPO_4 \cdot 2H_2O$ with 2-butanol, respectively. The small $VOHPO_4 \cdot 0.5H_2O$ crystallites transformed into single-phase $(VO)_2P_2O_7$ of high specific surface area under the reaction conditions of 1.5% *n*-butane, 17% O_2, and He (balance) at 663 K. In contrast, the catalyst formed from the large $VOHPO_4 \cdot 0.5H_2O$ crystallites assumed the form of particles having a double-layered structure, consisting of peripheral $(VO)_2P_2O_7$ and internal α_{II}-$VOPO_4$. As compared with the large $(VO)_2P_2O_7$, the small $(VO)_2P_2O_7$ showed high selectivity to maleic anhydride (∼78% at 663 K) and higher catalytic activity. Meanwhile, the catalyst with the double-layered structure exhibited moderate selectivity (∼70%). Since $(VO)_2P_2O_7$ is considered to be a selective phase for the selective oxidation of *n*-butane, the single-phase of $(VO)_2P_2O_7$ derived from the small-sized $VOHPO_4 \cdot 0.5H_2O$ crystallites is considered a reason for the high selectivity to maleic anhydride.

Keywords: Crystallite size; Microstructure; $VOHPO_4 \cdot 0.5H_2O$; *n*-Butane oxidation; Maleic anhydride

1. Introduction

Vanadium phosphate catalysts have been extensively studied for selective oxidation of *n*-butane to maleic anhydride (MA). Vanadyl pyrophosphate, $(VO)_2P_2O_7$, is a main active component, and is usually prepared from a precursor $VOHPO_4 \cdot 0.5H_2O$ [1–4]. It has been considered that the transformation from $VOHPO_4 \cdot 0.5H_2O$ to $(VO)_2P_2O_7$ proceeds through complex processes with dehydration, oxidation, and reduction in the reaction conditions [5–8], whereas the transformation proceeds topotactically in an inert atmosphere such as He and N_2 [9,10].

Abon et al. [5] demonstrated that a portion of $VOHPO_4 \cdot 0.5H_2O$ transformed into $(VO)_2P_2O_7$ through a topotactic dehydration and was partially oxidized into δ-$VOPO_4$, followed by reduction to $(VO)_2P_2O_7$ under the reaction gas (*n*-C_4H_{10}/O_2/He=1.6/18/80.4, VSHV=1500 h^{-1}) at 673 K. Hutchings et al. [6] observed the transformation under the flow of 1.5% *n*-butane in air using in situ Raman spectroscopy. During the temperature rise from 298 to 667 K, the intense peaks due to $VOHPO_4 \cdot 0.5H_2O$ completely disappeared at 643 K, and weak peaks attributed to $(VO)_2P_2O_7$ as well as α_{II}-, γ-, and δ-$VOPO_4$ appeared instead. Then, treatment at 667 K (final temperature) for 20 h brought about sharp, intense peaks attributable to $(VO)_2P_2O_7$. These observations indicate that the transformation from $VOHPO_4 \cdot 0.5H_2O$ to the resulting catalyst under the reaction gas proceeds through not only a simple dehydration process, but also complex reactions with oxidation and reduction of the catalyst.

Kiely et al. [7] revealed that the topotactic dehydration to $(VO)_2P_2O_7$ occurs preferentially at the periphery of the crystallites of $VOHPO_4 \cdot 0.5H_2O$, whereas $VOHPO_4 \cdot 0.5H_2O$ was initially oxidized to δ-$VOPO_4$ and then reduced to $(VO)_2P_2O_7$ in the interior of the crystallites for small size precursor crystallites (1–2 μm long and 0.03–0.1 μm thick).

* Corresponding author. Tel.: +81-11-706-4513; Fax: +81-11-706-4513.
E-mail address: oku@ees.hokudai.ac.jp (T. Okuhara).

1381-1169/$ – see front matter © 2004 Elsevier B.V. All rights reserved.
doi:10.1016/j.molcata.2004.03.054

They further demonstrated that variations in the preparation procedure of $VOHPO_4{\cdot}0.5H_2O$ lead to the catalysts with very different microstructure; $(VO)_2P_2O_7$ and some crystalline $VOPO_4$ (V^{5+}) phases are contained in various relative proportions [8]. This implies that the crystallite size of precursor greatly affects the crystalline phase and structure of the resulting catalyst.

In the present study, we investigate the influence of crystallite size of $VOHPO_4{\cdot}0.5H_2O$ on the microstructure of the catalyst, by employing two typical kinds of precursors of small-sized (av. 1 μm × 110 nm) and large-sized (av. 10 μm × 415 nm) crystallites prepared from $VOPO_4{\cdot}2H_2O$. Changes in the microstructures of the samples during the transformation from the precursors to the catalysts are systematically observed by X-ray diffraction, X-ray photoelectron spectra, redox titration, thermogravimetric analysis, N_2 adsorption–desorption isotherms, scanning electron microscopy, and transmission electron microscopy. Furthermore, their catalytic performances are discussed in relation to the microstructure of the catalyst particles.

2. Experimental section

2.1. Materials

2.1.1. $VOPO_4{\cdot}2H_2O$

$VOPO_4{\cdot}2H_2O$ serving as a raw material for $VOHPO_4{\cdot}0.5H_2O$ was prepared as follows. A mixture of V_2O_5 (24 g, Wako Pure Chem. Ind. Ltd.), aqueous 85% H_3PO_4 (223 g, Wako Pure Chem. Ind. Ltd.), and H_2O (577 cm^3) was refluxed for 24 h. The resulting precipitate was separated by filtration, washed with acetone, and dried at ambient temperature and pressure. The precipitant was identified as $VOPO_4{\cdot}2H_2O$, by XRD and IR.

2.1.2. $VOHPO_4{\cdot}0.5H_2O$

Two kinds of $VOHPO_4{\cdot}0.5H_2O$, with small and large crystallites, were prepared from the $VOPO_4{\cdot}2H_2O$. Small crystallites of $VOHPO_4{\cdot}0.5H_2O$ (denoted EP(small)) was prepared by intercalation-exfoliation-reduction process of $VOPO_4{\cdot}2H_2O$, which was previously reported [11]. A mixture of $VOPO_4{\cdot}2H_2O$ (1.0 g) and 2-butanol (50 cm^3, Wako Pure Chem. Ind. Ltd.) was heated stepwise with stirring at 303, 323, 343, and 363 K for 1 h at each temperature to yield a homogeneous yellow solution as the product of intercalation of 2-butanol into $VOPO_4{\cdot}2H_2O$ layers, followed by exfoliation [11]. After the addition of a small amount (5 mg) of $VOHPO_4{\cdot}0.5H_2O$ to the homogeneous solution, the solution was refluxed for 20 h (reduction) to form light blue precipitates, which were separated by centrifugation, washed with acetone, and dried at room temperature.

$VOHPO_4{\cdot}0.5H_2O$ having large-sized crystallites (denoted P(large)) were prepared by direct reduction of $VOPO_4{\cdot}2H_2O$ with 2-butanol. A mixture of $VOPO_4{\cdot}2H_2O$ (2.5 g) and 2-butanol (25 cm^3) was heated at 423 K for 15 h in a Teflon vessel (45 cm^3) equipped with a stainless steel jacket. The resulting solid was separated by filtration, washed with acetone, and dried at room temperature.

2.2. Characterization

XRD patterns of solid samples were measured by an XRD diffractometer (Miniflex, Rigaku) with Cu Kα radiation. The adsorption–desorption isotherms of nitrogen were measured at 77 K by an automatic adsorption apparatus (BELSORP 28SA, BEL Japan Inc.) after the precursors and catalysts were evacuated at 423 and 523 K, respectively. The surface areas and pore size distributions were calculated by the BET and DH methods, respectively. Thermogravimetric (TG) analysis was performed by a TG 8200 (Rigaku) in an He flow (50 $cm^3\ min^{-1}$) at 5 K min^{-1}.

Scanning electron microscope (SEM) images were taken by a S-2100 (Hitachi). Transmission electron microscope (TEM) images were taken with a H-800 (Hitachi) operating at 200 kV. The average oxidation number of V in the sample bulk was determined by a redox-titration method using $KMnO_4$ [12].

X-ray photoelectron spectra (XPS) were obtained by a Shimadzu XPS-7000 with Mg Kα radiation. All spectra were referenced to the carbon 1 s peak at a binding energy of 284.5 eV. $VOPO_4{\cdot}2H_2O$ and $(VO)_2P_2O_7$ were used as standard samples for V^{5+} and V^{4+}, respectively. The standard $(VO)_2P_2O_7$ was prepared by thermal treatment of EP(small) in a flow reactor at 663 K in He flow (20 $cm^3\ min^{-1}$) for 5 h. In order to avoid oxidation of the standard $(VO)_2P_2O_7$ surface with air, the sample was transferred from the reactor to the sample chamber of the XPS apparatus under an N_2 atmosphere. The oxidation number of the surface was estimated in the same manner as that reported in [5].

2.3. Dynamic transformation of $VOHPO_4{\cdot}0.5H_2O$ to catalyst and catalytic oxidation of n-butane

Transformation of $VOHPO_4{\cdot}0.5H_2O$ to corresponding catalyst was performed at 663 K in a flow reactor (Pyrex tube, 10 mm inside diameter) with a mixture of *n*-butane (1.5 vol.%), O_2 (17 vol.%), and He (balance) under atmospheric pressure. After the powder of $VOHPO_4{\cdot}0.5H_2O$ (0.68 g and 1.38 g for EP(small) and P(large), respectively) was placed in the reactor, the reactant gas was fed at a rate of 20 $cm^3\ min^{-1}$. Temperature was raised from room temperature to 663 K at a rate of 5 K min^{-1} and then maintained at 663 K. In order to observe the structural changes during the transformation, the samples were prepared while varying the treatment times (0.1, 0.5, 1, 3, 4, 25, and 300 h, which represent the time after the temperature reached 663 K).

In parallel with the transformation, the gas at the outlet of the reactor was analyzed by two on-line gas chromatographs. For *n*-butane and MA, an FID-GC (GC-8A, Shimadzu) equipped with Porapak QS columns (1 m) was

used. A high-speed GC (M200, Aera) equipped with Porapak Q and Molecular Sieves 5A columns was utilized for the analysis of CO, CO_2, and O_2.

After 200 h, stationary conversion of *n*-butane and selectivity to MA for the *n*-butane oxidation was attained (see results). In this paper, we call the samples after 300 h catalyst. The catalysts from EP(small) and P(large) are denoted EC(small) and C(large), respectively.

3. Results

3.1. Crystalline phases and microstructures of precursors and catalysts

Fig. 1 shows the bright field TEM images of the precursors and catalysts. The lateral lengths of EP(small) and P(large) were 1 and 5 μm, respectively. In the TEM images of both precursors, monolithic particles were observed (Fig. 1a and b). In contrast, mosaic patterns were observed inside the particles of both catalysts (Fig. 1c and d), indicating that the particles of the catalysts were polycrystalline; the patterns differed drastically depending on the catalyst. For EC(small) (Fig. 1c), at least two types of crystallytes were identified; one was oblong microcrystallite (ca. 50 nm) inside the particle and other was a distinct shell along the periphery whose thickness from the outer surface was estimated to be about 60 nm. The TEM image of C(large) revealed more complex microstructure (Fig. 1d). The particle of C(large) contained irregular shaped platelets, oblong microcrystallites showing strong contrast, and white circles in its inside. A distinct shell (ca. 70 nm thick) similar to that found in EP(small) was also observed in the periphery of C(large).

Fig. 2 shows SEM images of the precursors and catalysts. EP(small) was of thin and small leaf-like crystallite. The lateral lengths were distributed from 0.75 to 1.5 μm, with an average length of 1.0 μm (Fig. 2a). In contrast, P(large) showed a large platelet shape with an average lateral length of 10 μm (Fig. 2b). The shape and size of the particles of the catalysts were basically retained during the transformation, although, as described above, the interior of the catalyst particle changed drastically.

Table 1 summarizes the surface areas, lengths and thicknesses of particles, and the oxidation numbers of V in bulk and surface for the precursors and catalysts. Table 1 also lists the catalytic activity and selectivity to MA for the selective

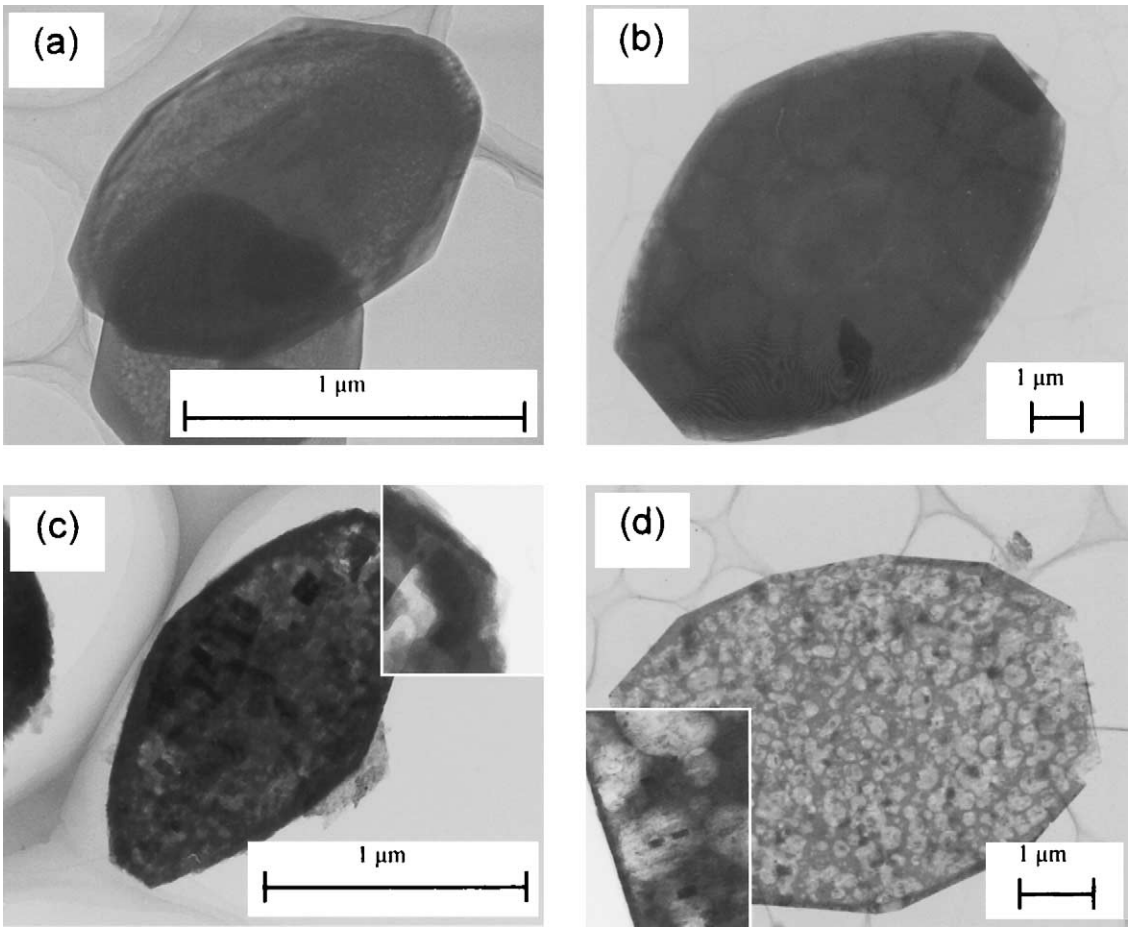

Fig. 1. TEM images of the precursors and catalysts: (a) EP(small); (b) P(large); (c) EC(small) and; (d) C(large) (insets in (c) and (d) are magnified images).

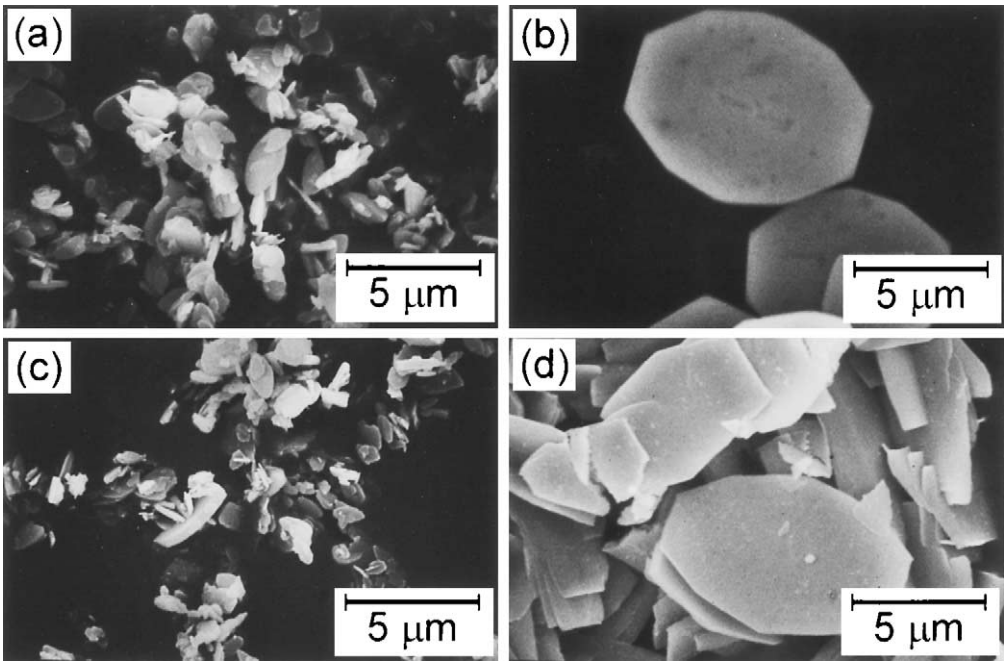

Fig. 2. SEM images of the precursors and the catalysts: (a) EP(small); (b) P(large); (c) EC(small); and (d) C(large).

oxidation of *n*-butane. The lateral lengths were estimated from the SEM images (Fig. 2). For the precursors, estimation of the thickness from the SEM images was difficult. In addition, Scherrer's equation could not be applied for the precursors, because the line-widths of XRD were too small (less than 0.05 deg. in 2θ) to allow estimation of the thickness. Thus, the thickness of the crystallites (t) of the precursor was estimated by Eq. (1) using a density (ρ; g cm^{-3}) which was calculated from the lattice constant and formula weight of $VOHPO_4{\cdot}0.5H_2O$, surface area (S; m^2 g^{-1}), and lateral length of the crystallites (L; μm).

$$\frac{2000}{t} + \frac{4}{L} = S\rho \quad (1)$$

Thickness of crystallites of P(large) was four times that of EP(small). Eq. (1) was not applied for the catalysts, because the particle of the catalysts consisted of poly crystals.

The oxidation numbers of V in the bulk and surface, which were estimated by redox titration and XPS, respectively, were close to 4.0 for both precursors. For the catalysts, the bulk oxidation number of V for C(large) greatly exceeded 4.0 ($V^{4.55+}$), whereas that for EC(small) was close to 4.0. However, a noteworthy finding is that two catalysts exhibited approximately equal surface oxidation numbers ($V^{4.23+}$). This inhomogeneity of the oxidation state of V between the bulk and surface for C(large) will be discussed in further detail later.

Table 1
Physical and chemical properties of precursors and catalysts and catalytic results of *n*-butane oxidation at steady states

Precursor and catalyst	S[a] (m^2 g^{-1})	L[b] (×10^3 nm)	t[c] (nm)	n of V^{n+d}		Rate[e] (10^{-4} mol g^{-1} h^{-1})	Selec. (Conv.)[f] (%)
				Bulk	Surface		
EP(small)[g]	8	0.75–1.5 (1.0)	110	4.01	4.00	–	–
EC(small)[h]	28	0.5–1.5 (0.8)		4.08	4.23	17 (0.58)	77.5 (50.9)
P(large)[g]	2	5.0–11.0 (10.0)	415	3.98	4.08	–	–
C(large)[h]	10	4.0–11.0 (8.0)	–	4.55	4.23	4 (0.39)	71.7 (43.2)
C(large)-He[i]	11	4.0–11.0 (8.0)		3.99	4.31	5 (0.48)	71.8 (42.8)

[a] Surface area measured after pretreatment at 423 K (precursor) or 523 K (catalyst) in a vacuum.
[b] Lateral length estimated from SEM. The figures in parenthesis denote average length.
[c] Thickness estimated from the surface area and the length.
[d] Average oxidation number of vanadium.
[e] The figures in parenthesis denote the specific activity per surface area (10^{-4} mol m^{-2} h^{-1}).
[f] The figures in parenthesis denote the conversion at which the selectivity was measured.
[g] Precursor ($VOHPO_4{\cdot}0.5H_2O$).
[h] After transformation under the reaction gas at 663 K for ca. 300 h.
[i] After treatment under He flow at 663 K for 4 h.

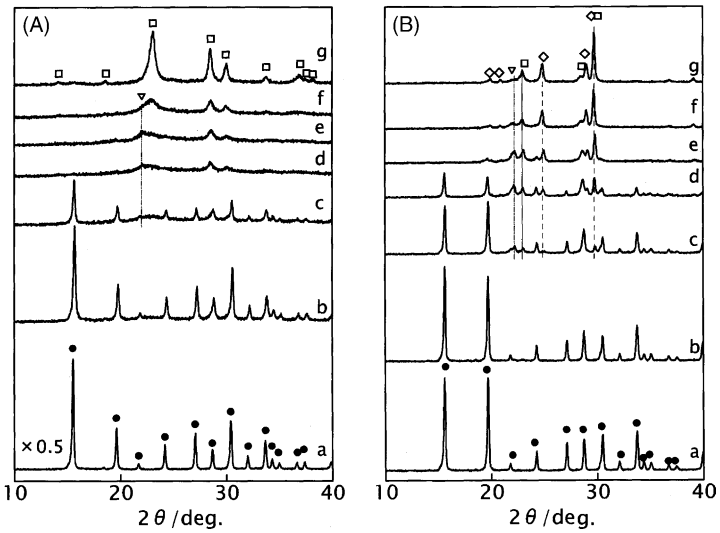

Fig. 3. Changes in XRD patterns of the samples during the transformation from precursors to catalysts: (A) EP(small)–EC(small) system and (B) P(large)–C(large) system. (a) 0 h; (b) 0.1 h; (c) 0.5 h; (d) 1 h; (e) 2 h; (f) 25 h and; (g) 300 h. The transformation was performed at 663 K with a mixture of *n*-butane 1.5%, O_2 17% and He (balance). Symbols ●, □, ▽, and ◇ in the figure denote $VOHPO_4{\cdot}0.5H_2O$, $(VO)_2P_2O_7$, δ-$VOPO_4$, and α_{II}-$VOPO_4$, respectively.

3.2. Changes in crystalline phases and structures during transformation from precursor to catalyst

The changes in crystalline phases with time during the transformation from the precursor to the catalysts were observed by XRD (Fig. 3). Both EP(small) and P(large) were confirmed to be well-crystallized $VOHPO_4{\cdot}0.5H_2O$ (Fig. 3A(a) and B(a)). For the EP(small)–EC(small) system (Fig. 3A), intensities of diffraction lines from $VOHPO_4{\cdot}0.5H_2O$ decreased rapidly with time. These diffraction lines completely disappeared at 1 h, and weak diffraction lines from $(VO)_2P_2O_7$ and δ-$VOPO_4$ phases appeared instead (Fig. 3A(d)). The diffraction lines from $(VO)_2P_2O_7$ became gradually intense with time, whereas those from δ-$VOPO_4$ finally disappeared. Note that after 300 h of the treatment (Fig. 3A(g)), only diffraction lines from $(VO)_2P_2O_7$ were observed.

The changes in crystalline phases for the P(large)–C(large) system (Fig. 3B) were drastically different from those for the EP(small)–EC(small) system. The diffraction lines from $VOHPO_4{\cdot}0.5H_2O$ also disappeared, but the disappearance took more time for P(large) than for EP(small). At 2 h (Fig. 3B(e)), new diffraction lines due to $(VO)_2P_2O_7$, δ-$VOPO_4$, and α_{II}-$VOPO_4$ became intense. After that time, the diffraction lines from δ-$VOPO_4$ gradually weakened, whereas those from α_{II}-$VOPO_4$ became intense with time. The diffraction lines from $(VO)_2P_2O_7$ were scarcely changed after 1 h of treatment. Contrary to the case of EC(small), α_{II}-$VOPO_4$ was a main phase for C(large), whereas $(VO)_2P_2O_7$ was a minor phase (Fig. 3B(g)).

Fig. 4 presents the changes in percentage of residual water in sample (Fig. 4A), bulk oxidation number of V (Fig. 4B), and surface area (Fig. 4C) as a function of treatment time. Each sample was prepared by treating of the precursor under the treatment conditions for planned times (see experimental section). In Fig. 4A, the percentage of the residual water in each sample was calculated from the data of TG analysis with Eq. (2).

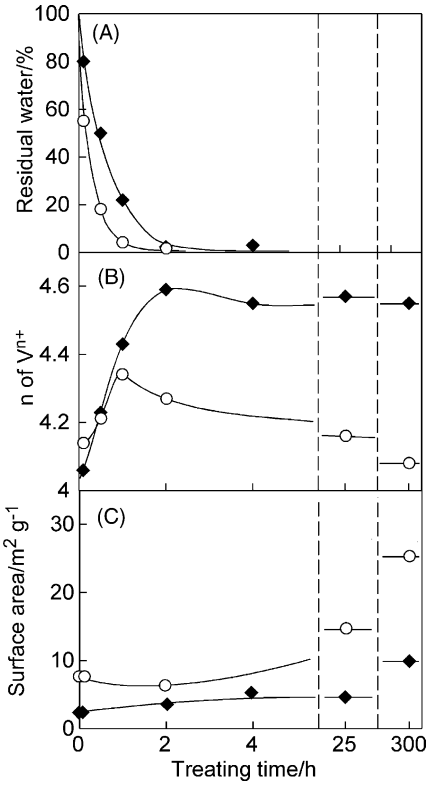

Fig. 4. Change in: (A) percent residual water in the sample; (B) average oxidation number of V and; (C) surface area as functions of treatment time. The transformation was performed at 663 K with a mixture of *n*-butane 1.5%, O_2 17%, and He (balance) ((○) EP(small)–EC(small) system and (◆) P(large)–C(large) system).

$$P_{\text{water}}(\%) = 100 - \frac{TW_{\text{loss}} - ((\Delta W / W_{300\,K}) \times 100)}{TW_{\text{loss}}} \times 100 \quad (2)$$

Here P_{water} is the percentage of residual water in the sample, ΔW is differential weight of the sample between 300 and 773 K as determined by TG analysis, and TW_{loss} (10.5%) is a theoretical weight loss for the dehydration calculated from Eq. (3).

$$2VOHPO_4 \cdot 0.5H_2O \rightarrow (VO)_2P_2O_7 + 2H_2O \uparrow \quad (3)$$

Since the reaction of Eq. (3) was completed by 723 K for both EP(small) and P(large) (Fig. 5), we adopted 773 K as the temperature of the termination of dehydration. For the EP(small)-EC(small) system, almost all water was released from the sample at 1 h, whereas complete dehydration of the P(large)–C(large) system took 2 h, demonstrating that the degradation of $VOHPO_4 \cdot 0.5H_2O$ for P(large) proceeded more slowly than that for EP(small). This is consistent with the results of XRD (Fig. 3). As shown in Fig. 5, the dehydration on EP(small) occurred from lower temperature than that on P(large).

As shown in Fig. 4B, in both systems the oxidation number increased rapidly with time at the initial stage. In the case of the EP(small)–EC(small) system, the oxidation number decreased with time through a maximum at 1 h ($V^{4.34+}$), and finally reached $V^{4.08+}$ at 300 h. In contrast, P(large) was more deeply oxidized than EP(small), where the maximum value was $V^{4.58+}$ (at 2 h), and subsequently, the bulk oxidation state scarcely changed ($V^{4.55+}$ at 300 h).

As shown in Fig. 4C, changes in the surface areas for EP(small)–EC(small) system were small in the initial few hours, and after 25 h, surface area increased greatly. The initial and final surface areas were 8.4 and 28.4 $m^2\,g^{-1}$, respectively. In the case of the P(large)–C(large) system, the surface area did not increase by 25 h, and the final value was 10.3 $m^2\,g^{-1}$ (at 300 h).

Fig. 6 shows the changes in mesopore size distributions of the samples with treatment time, where these distributions were estimated from the desorption branches of N_2 isotherms. For the EP(small)–EC(small) system (Fig. 6A), the samples treated within 2 h did not have mesopores, whereas mesopores with a peak of about 4 nm in diameter were formed at 25 h (Fig. 6A(c)). For the P(large)–C(large) system, no peak appeared in the mesopore region within 25 h, whereas the sample for 300 h; i.e. C(large), had mesopores with a peak around 4 nm in diameter (Fig. 6B(d)).

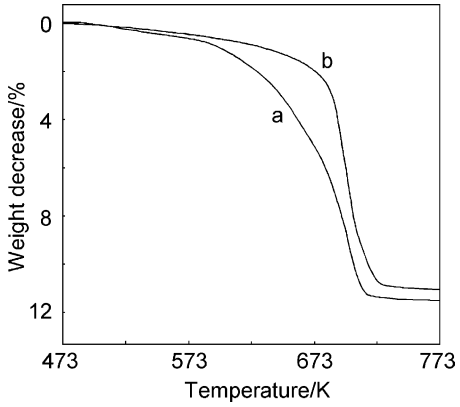

Fig. 5. TG curves of EP(small) and P(large) under He flow at heating rate of 5 K min^{-1}.

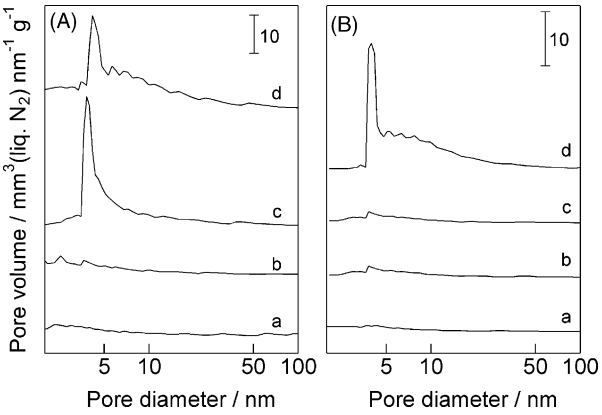

Fig. 6. Changes in mesopore size distributions of the samples as a function of treatment time. (A) EP(small)–EC(small) system and (B) P(large)–C(large) system: (a) 0 h; (b) 2 h; (c) 25 h and; (d) 300 h. The transformation was performed at 663 K with a mixture of *n*-butane 1.5%, O_2 17%, and He (balance).

3.3. Selective oxidation of n-butane

Fig. 7 shows the time course changes in the selective oxidation of *n*-butane at 663 K, where the catalyst weights are 0.68 and 1.38 g for EP(small) and P(large), respectively. For the EP(small)–EC(small) system, the conversion gradually

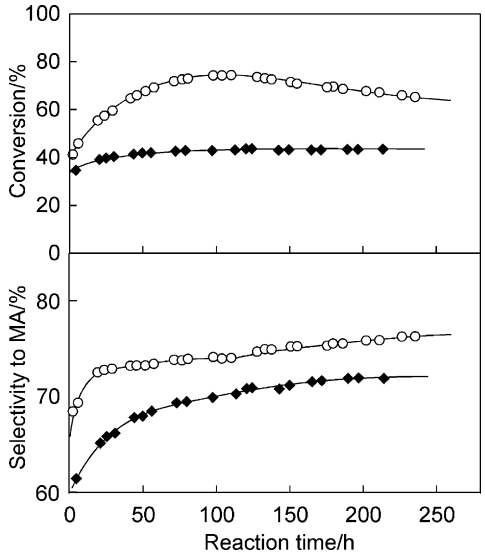

Fig. 7. Time course changes in oxidation of *n*-butane over the catalysts formed from (○) EP(small)) (W/F = 0.85 kg h mol^{-1}) and (◆) P(large) (W/F = 1.7 kg h mol^{-1}). The reaction was performed at 663 K with a mixture of *n*-butane 1.5%, O_2 17%, and He (balance).

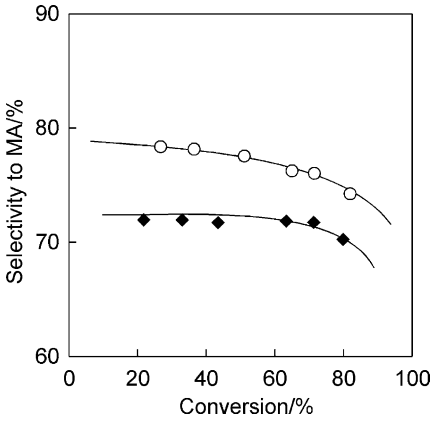

Fig. 8. Changes in selectivity to maleic anhydride as a function of conversion of *n*-butane: (○) EC(small)) and (◆) C(large). The reaction was performed at 663 K with a mixture of *n*-butane 1.5%, O_2 17%, and He (balance). The data were collected after 300 h of reaction.

increased until about 100 h, and then decreased slowly to a stationary value after 200 h. Selectivity to MA increased rapidly at initial 20 h, and then increased slowly. In contrast, for the P(large)–C(large) system, the changes in conversion were small, whereas the selectivity increased with the lapse of time, and stable selectivity was obtained after 150 h.

Fig. 8 shows the selectivity to MA plotted against the conversion, in which flow rates were changed after the stationary conversions and selectivities were obtained. The selectivity for EC(small) was higher than that for C(large) over the entire range of the conversions. As shown in Table 1, the activity of EC(small) was about four times that of C(large), whereas the specific activity (per unit surface area) was similar. The selectivity around 50% conversion was 78 and 72% for EC(small) and C(large), respectively.

4. Discussion

4.1. Influence of crystallite size of precursors on crystalline phases and microstructures of the catalysts

The transformation from $VOHPO_4{\cdot}0.5H_2O$ to $(VO)_2P_2O_7$ proceeds through complex processes with dehydration, oxidation, and reduction in the reaction conditions [5–8]. Kiely et al. [7] demonstrated that a direct topotactic transformation from $VOHPO_4{\cdot}0.5H_2O$ to $(VO)_2P_2O_7$ occurs at the periphery of the crystallite, whereas $VOHPO_4{\cdot}0.5H_2O$ initially transforms epitaxially into δ-$VOPO_4$ in the interior of the crystallite, followed by reduction of δ-$VOPO_4$ into $(VO)_2P_2O_7$. In addition, they further reported that the catalysts, which were derived from $VOHPO_4{\cdot}0.5H_2O$ prepared by different preparation methods, contained $(VO)_2P_2O_7$ and some crystalline $VOPO_4$ (V^{5+}) phases in various relative proportions [8]; $VOHPO_4{\cdot}0.5H_2O$ (5 μm × 1 μm) prepared in an aqueous medium transformed mainly into α_{II}-$VOPO_4$, while single $(VO)_2P_2O_7$ phase was formed from $VOHPO_4{\cdot}0.5H_2O$ (~1 μm × 0.1 μm) prepared by reduction of $VOPO_4{\cdot}2H_2O$. Although two precursors had different chemical and physical properties such as crystallinity and morphology, there findings made us suppose that the crystallite size of the precursor affected the microstructure of the catalyst.

In the present study, we used two typical precursors, EP(small) and P(large), having different particle sizes; that is, 1 μm (length) × 110 nm (thickness) and 10 μm (length) × 415 nm (thickness). As shown in Fig. 3, EP(small) transformed into pure $(VO)_2P_2O_7$ phase (EC(small)), whereas the catalyst (C(large)) containing mainly α_{II}-$VOPO_4$ phase was formed from P(large). Since the two precursors had almost the same P/V atomic ratio and oxidation states in the bulk and surface (Table 1), and were well-crystallized $VOHPO_4{\cdot}0.5H_2O$ (Fig. 3), the difference in crystallite size between two precursors can be considered the cause of the difference in the crystalline phases formed in the catalysts.

As listed in Table 1, the bulk oxidation number of V for EC(small) was nearly 4.0, and the surface oxidation number slightly exceeded 4.0+, being $V^{4.2+}$. Since XPS can be applied only to surface layers, these results indicate that only the top few surface layers of EC(small) were oxidized during the steady-state reaction. The selective oxidation of *n*-butane over $(VO)_2P_2O_7$ has been accepted to proceed via a redox mechanism involving V^{4+} and V^{5+} at a few surface layers [13–15]; thus, the surface layers at the steady-state reaction would contain the V^{5+} species to some extent. The surface oxidation state of EC(small) was consistent with this concept. In the case of C(large), the surface oxidation state was similar to that of EC(small), whereas the catalyst bulk was deeply oxidized ($V^{4.55+}$). This result indicates that the oxidized phases such as α_{II}-$VOPO_4$ and δ-$VOPO_4$ for C(large) existed mainly in the internal particle. Kiely et al. [7] demonstrated that the dehydration of $VOHPO_4{\cdot}0.5H_2O$ to $(VO)_2P_2O_7$ proceeded preferentially at the periphery of the crystallites in the initial stage, and, in contrast, the internal crystallite of $VOHPO_4{\cdot}0.5H_2O$ tended to transform into α_{II}-$VOPO_4$. Our present results revealed that the oxidation of $VOHPO_4{\cdot}0.5H_2O$ to α_{II}-$VOPO_4$ was almost completely suppressed when the small size precursor (1 μm long and 110 nm thick) was employed. The reason why the large-sized catalyst particle was more oxidized than the small catalyst particle will be discussed in the next section.

As shown in Fig. 1c, the internal particle of EC(small) was made up of oblong microcrystallites (ca. 50 nm). In consideration of the XRD pattern (Fig. 3A(g)) and the bulk oxidation number (Table 1) for EC(small), the crystalline phase of these oblong microcrystallites was ascribed to $(VO)_2P_2O_7$. Meanwhile, the interior of C(large) contained the irregular shaped platelets and some oblong microcrystallites. In addition, many white circles were observed in the TEM image of C(large). In consideration of the bulk oxidation number and XRD result, about half of V presented as the oxidized phases, mainly α_{II}-$VOPO_4$, and the others as $(VO)_2P_2O_7$ in

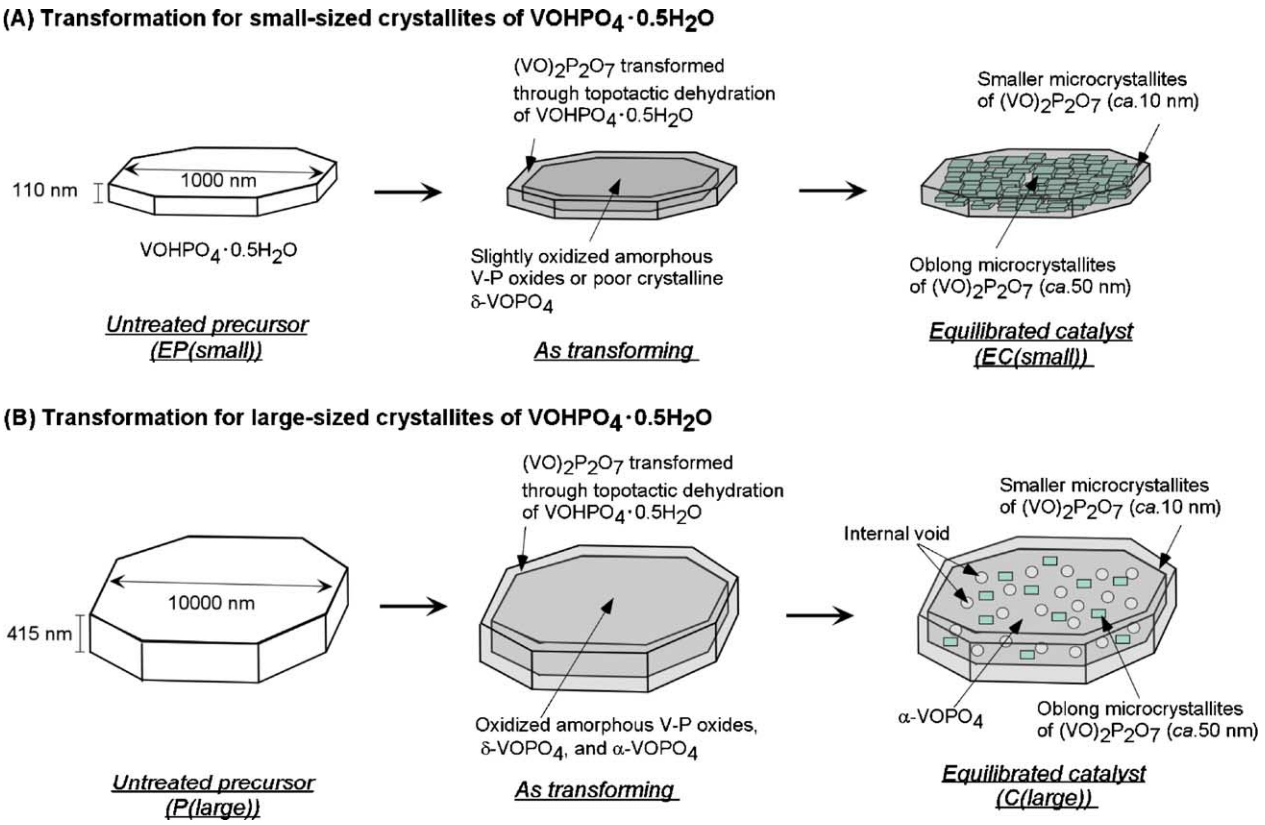

Fig. 9. Schematic models of particle structures during the transformation for (A) EP(small) and (B) P(large).

C(large). The difference in the contrast between $(VO)_2P_2O_7$ and α_{II}-$VOPO_4$ in a TEM image is expected to be small, because the density of $(VO)_2P_2O_7$ estimated from the lattice constant and molecular weight is almost the same as that of α_{II}-$VOPO_4$. Thus, white circles present in the internal C(large) are unlikely to be $(VO)_2P_2O_7$ or α_{II}-$VOPO_4$. Therefore, the observed white circles in C(large) can be associated with internal voids. Although uncertainty remains in relation to which of the oblong microcrystallites and the irregular shaped platelets are $(VO)_2P_2O_7$ or α_{II}-$VOPO_4$ in C(large), similarity of the oblong shape to that of EC(small) suggests that the crystalline phase of the oblong microcrystallites is assigned to $(VO)_2P_2O_7$.

On the basis of these results, schematic models of the catalyst particles for EC(small) and C(large) are depicted in Fig. 9.

4.2. Changes in microstructure during transformation

Under flow of helium, the transformation from $VOHPO_4 \cdot 0.5H_2O$ to $(VO)_2P_2O_7$ at 663 K was completed within 1 h for both EP(small) and P(large) (data not shown). However, as shown in Fig. 3, transformation of EP(small) to $(VO)_2P_2O_7$ in the presence of the reaction gas proceeded slowly, whereas P(large) transformed into mainly α_{II}-$VOPO_4$. These results indicate that the transformation in the presence of the reaction gas took place through processes involving dehydration, oxidation, and reduction, and the crystallite size of the precursor obviously dominates these processes.

In the case of the EP(small)–EC(small) system, weak diffraction lines due to $(VO)_2P_2O_7$ and δ-$VOPO_4$ arose at 1 h of treatment, instead of disappearance of $VOHPO_4 \cdot 0.5H_2O$ (Fig. 3A(d)). Since the diffraction lines were very weak for the sample at 1 h, amorphous V-P oxides are also included. As shown in Fig. 4A and B, the bulk oxidation number of V increased as residual water decreased in the initial stage. This relationship suggests that, in the initial stage, the oxidized phases were formed by direct transformation of $VOHPO_4 \cdot 0.5H_2O$. Abon et al. [5] demonstrated that a portion of $VOHPO_4 \cdot 0.5H_2O$ is oxidized to δ-$VOPO_4$ under the reaction gas. Kiely et al. [7] speculate that, in consideration of the structure of $VOHPO_4 \cdot 0.5H_2O$, water molecules of $VOHPO_4 \cdot 0.5H_2O$ are released to the direction along the layers when the direct dehydration of $VOHPO_4 \cdot 0.5H_2O$ occurs, and further claimed that this dehydration is achieved within an extremely short time in the periphery of the precursor crystallites [7]. Thus, the temporarily existing oxidized amorphous phases in the particle of EP(small)–EC(small) system are reasonably supposed to be located inside the particle rather than in surface layers.

As shown in Fig. 4C, the surface area did not change at all in the initial few hours for the EP(small)–EC(small) system and no peak was present in the mesopore region (Fig. 6A(a)

and A(b)), indicating that the particles did not cleave at this stage, and the inside of the particle could not come into direct contact with the surrounding gases. Thus, $VOHPO_4{\cdot}0.5H_2O$, which exists inside the particle, is considered to be oxidized by oxygen diffused from the surface.

After 25 h, since the surface area increased (Fig. 4C) and a peak at 4 nm in the mesopore region appeared (Fig. 6A(c)), the particles of EP(small)–EC(small) system had been cracked. This probably allowed the reduction of the oxidized phases existing originally inside the particle, by direct contact with *n*-butane. As a result, the catalyst particle formed from EP(small) was reduced to about $V^{4.0+}$. The mode of the transformation from the small $VOHPO_4{\cdot}0.5H_2O$ crystallites is illustrated in Fig. 9A.

In the case of large crystallites (P(large)), the water molecules still remained in the sample particle at 1 h (Fig. 4A), and $VOHPO_4{\cdot}0.5H_2O$ was also detected by XRD (Fig. 3B(d)), indicating that dehydration from the large-sized $VOHPO_4{\cdot}0.5H_2O$ particle was slower than that from the small-sized particle. The TG analysis in He flow (Fig. 5) supports this finding.

As mentioned above, the direct dehydration of $VOHPO_4{\cdot}0.5H_2O$ would occur preferentially in the edge of the crystallites. A reasonable assumption is that this dehydration proceeds to nearly the same depth from the surface independent of the crystallite size. The TEM images of the catalysts (Fig. 1d and e) demonstrate that the thickness of the shell, which would be formed by direct dehydration, in C(large) (ca. 70 nm) is similar to that for EP(small) (ca. 60 nm). Consequently, at the initial stage the particles of the P(large)–C(large) system contain a greater amount of $VOHPO_4{\cdot}0.5H_2O$ inside the crystallites. Since $VOHPO_4{\cdot}0.5H_2O$ can be oxidized directly to δ-$VOPO_4$ [5], the large-sized precursor was deeply oxidized, in comparison with the small precursor. δ-$VOPO_4$ is reported to transform progressively to the more stable α_{II}-$VOPO_4$ phase, and α_{II}-$VOPO_4$ is not further reduced to $(VO)_2P_2O_7$ under the reaction conditions [7,16]. Thus, we conclude that the δ-$VOPO_4$ phase confined inside the P(large) particle gradually transformed to stable α_{II}-$VOPO_4$, which was no longer reduced, and this is a reason why the large-sized catalyst particles remained in the high oxidation state ($V^{4.55+}$). The process of transformation in the large-sized particle is depicted in Fig. 9B.

4.3. Influence of the microstructure of the catalysts on selectivity in the selective oxidation of n-butane

Shomoda et al. [17] reported that α_{II}-$VOPO_4$ yielded only 20–30% selectivity towards MA, whereas $(VO)_2P_2O_7$ yielded about 70% selectivity. In the present study, the small-sized precursor (EP(small)) transformed into pure $(VO)_2PO_7$ phase, which accounts for the high selectivity of EC(small). Meanwhile, surprisingly, although the main phase of C(large) was α_{II}-$VOPO_4$, C(large) showed moderate selectivity to MA (∼70%). The selective oxidation of *n*-butane over $(VO)_2P_2O_7$ proceeds via a redox mechanism at a few surface layers [13–15]. As mentioned in the previous section, the surface oxidation state of C(large) was almost the same as that of EC(small), suggesting that the two catalysts are of similar structure near the surface. This is a reason for the moderate selectivity of C(large), in spite of the main phase of α_{II}-$VOPO_4$.

We have further examined the influence of the α_{II}-$VOPO_4$ phase, which is present inside the particle of C(large). To avoid the formation of V^{5+} phase, precursor P(large) was dehydrated in He instead of the reactant mixture, and the resulting sample, C(large)-He, was shown to have a surface area of $10\,m^2\,g^{-1}$ and a crystallite shape similar to that of C(large) (Table 1). The oxidation number of V of the catalyst bulk was determined to $V^{3.99+}$. In addition, the surface oxidation state of C(large)-He was the same as that of C(large). Accordingly, XRD studies have revealed that C(large)-He contains a pure phase of $(VO)_2P_2O_7$. The catalytic activity of C(large)-He is slightly higher than that of C(large) (Table 1), and correspondingly, its selectivity is similar to that of C(large). These results indicate that the influence of α_{II}-$VOPO_4$ that is located inside the particles on the catalytic property is not very large, and therefore, the essential functions of these catalysts are governed by the structure of the surface layers. Recently Bordes and Duvauchelle [18] inferred that a mosaic texture was formed during the dehydration process of $VOHPO_4{\cdot}0.5H_2O$ to $(VO)_2P_2O_7$ and presumed that the intercrystallite boundaries play an important role in the selective oxidation of *n*-butane. The influences of the microstructure of the catalyst crystallites on the activity and selectivity must be critical, and these remain issues to be solved.

5. Conclusion

The present study clearly demonstrates that crystallite size of the precursor $VOHPO_4{\cdot}0.5H_2O$ greatly affects crystallite phases and microstructure of the catalyst formed under the reaction conditions. The small size crystallites of $VOHPO_4{\cdot}0.5H_2O$ (1 μm (length) × 110 nm (thickness)) transform into pure $(VO)_2P_2O_7$. In contrast, the catalyst in which the inside of the particle is mainly α_{II}-$VOPO_4$ is formed from large-sized crystallites of $VOHPO_4{\cdot}0.5H_2O$ (10 μm (length) × 415 nm (thickness)).

The catalyst formed from the small-sized $VOHPO_4{\cdot}0.5H_2O$ crystallites shows high selectivity to maleic anhydride (∼78%), because of the presence of pure $(VO)_2P_2O_7$ as well as the highly dispersed V^{5+} species on the surface. The catalyst obtained from the large-sized $VOHPO_4{\cdot}0.5H_2O$ crystallites exhibits moderately high selectivity (∼70%), in spite of the main phase of α_{II}-$VOPO_4$. The similarity in surface structure independent of the crystallite size is responsible for the moderately high selectivity for the catalyst formed from the large-sized crystallites of $VOHPO_4{\cdot}0.5H_2O$.

Acknowledgements

This work was partially supported by the New Energy and Industrial Technology Development Organization (NEDO). This work was also supported by a Grant-in-Aid for Scientific Research from the Ministry of Education, Science, Sports, and Culture, Japan.

References

[1] G. Centi, F. Trifirò, J.R. Ebner, V.M. Franchetti, Chem. Rev. 88 (1988) 55.
[2] B.K. Hodnett, Catal. Rev. Eng. 17 (1985) 373.
[3] S. Albonetti, F. Cavani, F. Trifirò, Catal. Rev. Sci. Eng. 38 (1996) 413.
[4] F. Trifirò, F. Cavani, J.A. Horsley, S.R. Vatcha, Selective Partial Oxidation of Hydrocarbons and Related Oxidations, Catalytica Studies Division 4193 So, Mountain View, CA (1994).
[5] M. Abon, K.E. Bere, A. Tuel, P. Delichere, J. Catal. 156 (1995) 28.
[6] G.J. Hutchings, A. Desmartin-Chamel, O. Oliver, J.C. Volta, Nature 348 (1994) 41.
[7] C.J. Kiely, A. Burrows, G.J. Hutchings, K.E. Bere, J.C. Volta, A. Tuel, M. Abon, Faraday Discuss. 105 (1996) 103.
[8] C.J. Kiely, A. Burrows, S. Sajip, G.J. Hutchings, M.T. Sananes, A. Tuel, J.C. Volta, J. Catal. 162 (1996) 31.
[9] J.W. Johnson, D.C. Johnston, A.J. Jacobson, J.F. Brody, J. Am. Chem. Soc. 106 (1984) 8123.
[10] E. Bordes, P. Courtine, J. Solid State Chem. 55 (1984) 270.
[11] N. Yamamoto, N. Hiyoshi, T. Okuhara, Chem. Mater. 14 (2002) 3882.
[12] B.K. Hodnett, P. Permanne, B. Delmon, Appl. Catal. 6 (1983) 231.
[13] M. Pepera, J.L. Callahan, M.J. Desmond, E.C. Milberger, P.R. Blum, N.J. Bremer, J. Am. Chem. Soc. 107 (1985) 4883.
[14] T. Okuhara, M. Misono, Catal. Today 16 (1993) 61.
[15] G. Koyano, T. Okuhara, M. Misono, J. Am. Chem. Soc. 120 (1998) 767.
[16] F.B. Abdelouahab, R. Olier, N. Guilhaume, F. Lefebvre, J.C. Volta, J. Catal. 134 (1992) 151.
[17] T. Shimoda, T. Okuhara, M. Misono, Bull. Chem. Soc. Jpn. 58 (1985) 2163.
[18] N. Duvauchelle, E. Bordes, Catal. Lett. 57 (1999) 81.